RSC Advances

ROYAL SOCIETY OF CHEMISTRY

www.rsc.org/advances

Cite this: DOI: 10.1039/c0xx00000x

www.rsc.org/xxxxxx

ARTICLE TYPE

High photoactive heterojunction based on g-C_3N_4 nanosheets decorated with dendritic zinc (II) phthalocyanine through axial coordination and its ultrasensitive enzyme-free sensing for choline

Hong Dai [a*], Shupei Zhang [a], Guifang Xu [a], Yiru Peng [a], Lingshan Gong [a], Xiuhua Li [a], Yilin Li [a], Yanyu Lin [a,b], Guonan Chen [b*]

Received (in XXX, XXX) Xth XXXXXXXXX 20XX, Accepted Xth XXXXXXXXX 20XX

DOI: 10.1039/b000000x

A heterojunction with excellent photocatalytic performance based on graphene-like carbon nitride (g-C_3N_4) nanosheets and dendritic zinc (II) phthalocyanine was firstly proposed. Herein, the g-C_3N_4 with excellent photo-activity and high nitrogen content was readily available functional material. The g-C_3N_4 acted as an easy electron pair donor for dendritic zinc (II) phthalocyanine through axial coordination, forming the p-n heterojunction. Then by taking advantages of distortion of dendritic zinc (II) phthalocyanine, the spatial charge separation of photo-generated charge carriers in this metal macrocycles achieved high efficiency, resulting in the enhanced photo-to-electric conversion efficiency. Therefore, the optoelectronic sensing device based on the heterojunction led to the obvious enhanced photocurrent, and made it a promising candidate for establishing photoelectrochemical biosensors. Moreover, the p-n heterojunction was successfully applied to the detection of choline with wide linear range from 10 nM to 5 μM, which could be oxidated by the photo-generated holes. Along with these attractive features, the as-proposed biosensor also displayed a remarkable specificity against other interferents and could be successfully used for detecting choline in the real samples. The heterojunction with prominently enhanced photoelectronic properties provids a promising format for the future development of photoelectrochemical biosensors.

Photoelectrochemistry is a newly emerging yet dynamically developing analytical method which displays promising analytical applications and has attracted considerable interests.[1-2] Because of its different forms of energy for excitation and detection, the photoelectrochemical (PEC) analytical methods not only possess well temporal and spatial controlled, but also have high sensitivity with low background signals.[3-7] In recent years, the fascinating inorganic semiconductor nanostructures and rutheniumbipyridine have been widely regarded as attractive candidate photosensitizers for photoelectric applications resulting from their optical and electronic properties.[4,8-10] Recently, g-C_3N_4 nanosheets, an appealing class of two-dimensional semi-conductive layered nanomaterials, has been explored for various applications, especially in the fields of visible light photo-catalysis and photodegradation attributing to its large specific surface area, short diffusion length, high chemical stability and appealing electronic structure with a band gap of 2.7 eV.[11-13] In addition, the high nitrogen content in the g-C_3N_4 frameworks plays an essential role on the high photoelectric conversion efficiency, where the nitrogen atoms affect the spin density and the charge distribution of carbon atoms, including an activation region on the layer surface.[14] On one hand, the band gap of g-C_3N_4 between the conduction band (CB) and the valence band (VB) could be opened, because the nitrogen causes the Fermi level to shift above the Dirac point, and the density of the states near the Fermi level is suppressed.[15-16] However, the photo-to-current conversion efficiency of bare g-C_3N_4 is still cursed by the high recombination rate of photo-generated electron-hole pairs and the quantum efficiency for the pristine semiconductor.[13,17]

To improve the photo-to-current conversion efficiency of g-C_3N_4, dendritic zinc (II) phthalocyanine (DZP) bearing poly (aryl benzyl ether) dendritic substituents was employed in this text. Due to the excellent thermal and photochemical stability, phthalocyanines are obviously versatile and possible to change the central atom and to introduce substituents in the peripheral and axial positions, leading to the possibility to tune their applications as photosensitizers for photodynamic therapy.[18-19] And yet, the traditional phthalocyanines always suffer from molecular aggregation attributed to their intrinsic large π-conjugation, resulting in shortening triplet state lifetime and reducing the quantum yield.[20] To resolve this problem, in this paper, DZP was synthesized with hydrophilic stability to avoid aggregation. The dendritic architectures of DZP employed in the photoelectrochemical system could achieve antenna effect, which could conduce a larger light-harvesting system and facilitate the photons absorption in the visible region.[21] Even though dendrimeric phthalocyanine has such attracted much attention, till now, few groups have utilized dendrimeric phthalocyanine to establish photoelectrochemical sensor. Herein, DZP was found could couple with g-C_3N_4 nanosheets through axial coordination to

make this compound distorted, where g-C_3N_4 as Lewis base exhibited strong adsorption capacity towards the zinc ion of DPZ. The electrostatic repulsive force also existed between the electronegative g-C_3N_4 and DZP, which then induced phthalocyanine ring to be distorted, and the Lewis acidity of the Zn (II) to be stronger, bringing about the stronger axial coordination.[18] Additionally, the formation of p-n heterojunctions between n-type g-C_3N_4 and an organic p-type charge transport material DZP could realize the low recombination rate of the electron-hole pairs and lead to the efficient charge separation process. Consequently, by using the stronger Lewis acidity of Zn (II) in the non-planar Zn (II) complex of distorted DZP and g-C_3N_4, a supermolecular electron donor-acceptor assembly could be constructed. [22-23] And the photovoltaic devices based on the p-n heterojunctions formed by g-C_3N_4 and DZP could not only facilitate the charge transfer, but also improve the performance of the optoelectronic systems, resulting in the enhanced photocurrent and making it a promising candidate for establishing photoelectrochemical biosensors. To evaluate the application of the excellent photoactive nanocomposites in analysis detection, choline (Ch), a dietary essential nutrient involved in several body functions, as a research sample was introduced into the determination.

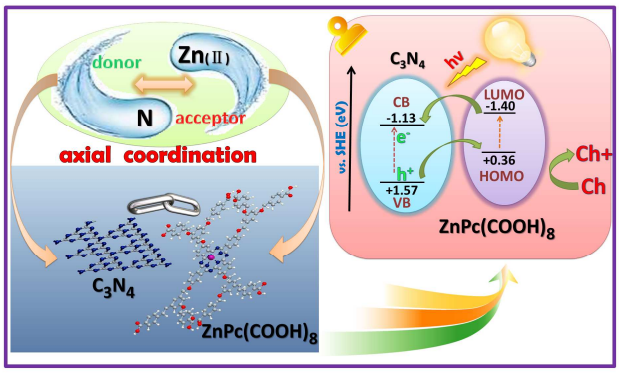

Scheme 1 Schematic illustration of the axial coordination between g-C_3N_4 and DZP and schematic model for the PEC process of g-C_3N_4/DZP composites under visible light.

In this text, our group firstly developed a non-enzyme PEC biosensor for direct, rapid and sensitive detection of Ch based on the Ch oxidation by photo-generated holes, thus resulting in obviously enhanced photocurrent. The detection result indicated that the g-C_3N_4/DZP axial coordinated composites provided a promising method for the future development of other PEC biosensors and a versatile tool in determining low abundance analyte in bioanalysis and clinical biomedicine. The electrode decorated with high charge separation efficiency g-C_3N_4/DZP compound for non-enzyme PEC determination of Ch was depicted in Scheme 1. DZP was coupled with g-C_3N_4 nanosheets through axial coordination, where the nitrogen in g-C_3N_4 acted as electron donor and the zinc ion of DZP was regarded the electron acceptor. The energy levels of the LUMO and HOMO of DZP just could match with that case of g-C_3N_4 nanosheets.[24] Hence, when the visible light irradiated the axial coordinative compound, the holes emanated from the VB of g-C_3N_4, then they injected into the HOMO of the DZP, resulting in the high efficiency of the charge separation. Afterward, since Ch could be oxidized by the holes, it could act as the effective electron donor for scavenging of holes, leading to the inhibition of the electron-hole recombination, then the photocurrent intensity enhanced dramatically.

As shown in Fig.1, open-circuit voltage-decay measurements were conducted investigate the recombination kinetics of the structure. The open-circuit voltage after stopping the illumination presented the following the technique as reported previously. And it could be analyzed using the approximation derived by Bisquert. The photovoltage decay rate directly related to the electron lifetime by the following equation:[25-26]

$$\tau = \frac{k_B T}{e}\left(\frac{dV_{oc}}{dt}\right)^{-1} \quad (1)$$

Here, τ is the potential dependent lifetime, k_B is Boltzmann's constant, T is the temperature in K, e is the charge of a single electron, and V_{oc} is the open-circuit voltage at time t. Fig.1B was the plot of the response time which obtained by applying equation 1 to the data in Fig.1A. By a comparison, the response time data for g-C_3N_4/DZP nanocomposite was significantly longer, which resulted from that the energy levels of the LUMO and HOMO of DZP just could match with that case of g-C_3N_4 nanosheet. The result exhibited long life-lived and efficient charge separation was achieved in the axial coordination composites.[27] The effective charge separation led to improved IPCE in g-C_3N_4/DZP, which exhibited in Fig. S4. Therefore, g-C_3N_4/DZP compound possessed a promising application for PEC sensors.

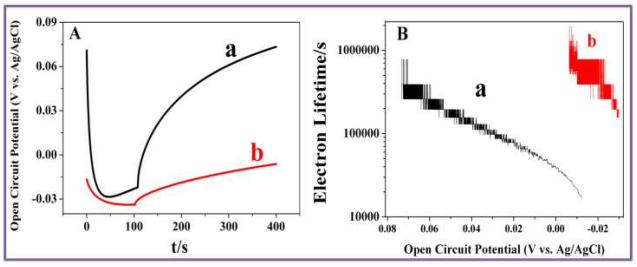

Fig.1 (A) V_{oc} time profile of g-C_3N_4(a), g-C_3N_4/DZP(b);(B) Electron life-time measurements determined from the V_{oc} decay in dark by applying eq1, g-C_3N_4(a), g-C_3N_4/DZP(b).

The dendritic zinc phthalocyanine which was artificial light harvesting system, possessed the special dendritic architecture. Due to the periphery of dendritic macromolecules acting as the energy absorbing and electron transferring antenna, the light harvesting property of DZP was improved dramatically. The photo-physical properties of DZP were characterized by fluorescence spectroscopy in the Figure S5A. Upon excitation at 290 nm, the fluorescence emission spectra of water-soluble DZP in water was at 678 nm, and the strong fluorescent intense was observed obviously without the aid of surfactants, which was unprecedented. Figure S5B showed the optical absorption spectra of g-C_3N_4 (a) and g-C_3N_4/DZP (b) in aqueous solution, normalized to their most intense absorption bands. The g-C_3N_4 had relatively obvious UV absorption peak at 231 nm and 328 nm, respectively. After the g-C_3N_4 was functionalized by DZP, the changes

were observed in spectral. Compared with the pure g-C_3N_4, the absorption bands of the composites were characterized at 223 and 321nm with 7-8 nm blue shifts, proving that the axial coordination between DZP and g-C_3N_4 successfully formed. Then the axial coordination bond between DZP and g-C_3N_4 underwent charger separation and made the composites to construct supermolecular assemblies of light harvesting and charge separation units, which provided potential perspective for the development of efficient light energy conversion systems. The result in accord with that of Fig. S6.

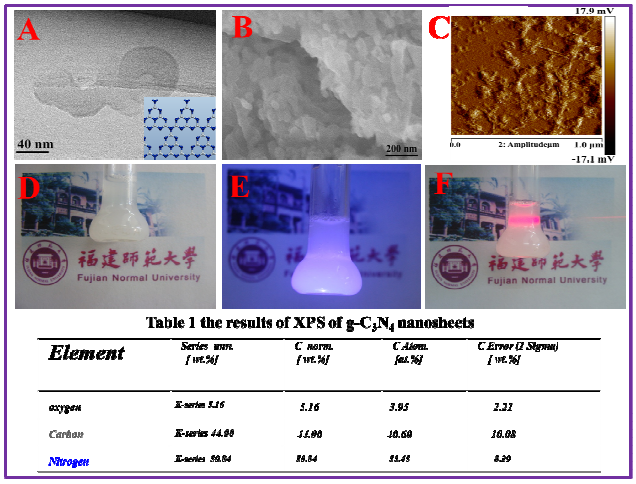

Table 1 the results of XPS of g-C_3N_4 nanosheets

Element	Series norm. [wt.%]	C norm. [wt.%]	C Atom. [at.%]	C Error (2 Sigma) [wt.%]
oxygen	K-series 5.16	5.16	3.95	2.21
Carbon	K-series 44.80	44.80	50.60	16.08
Nitrogen	K-series 50.04	50.04	51.45	8.29

Fig.2 (A) TEM image of g-C_3N_4, (B) SEM image of g-C_3N_4, (C) AFM image of g-C_3N_4 , (D) the photos of diluted g-C_3N_4 nanosheets solution under white light and 390nm visible light (E), (F) the photo of the Tyndall phenomenon of the g-C_3N_4. Table 1 The results of XPS of g-C_3N_4 nanosheets.

The TEM image of g-C_3N_4 (Figure 2A) showed distinctly layered structure, predicating that g-C_3N_4 was consisted of graphitic plans stacking. The planes were constructed from tri-s-triazine units displayed in the inset of Figure 2A. The SEM image of g-C_3N_4 showed in Figure 2B suggested the nanosheets was loose and soft, and the basic unit was sheets. The large 2D aromatic surface of g-C_3N_4 makes it an ideal substrate in potential use including biosensing, photoelectrochemsitry, and electroanalysis, etc. To gain the insight into the morphology and thickness of the nanosheets, the atomic force microscopy (AFM) image was recorded in Figure 2C. It described the topographic heights of these sheets with the range between 0.3 nm and 8.1 nm, suggesting that g-C_3N_4 consist of only several layers of nanosheet. Additionally, the high water-dispersity was showed in Figure 2 (D, E, F). Especially, the obvious Tyndall phenomenon suggested that the particles of the g-C_3N_4 in solution were stable and distributed quite uniformly in water. The analytical results of XPS of g-C_3N_4 nanosheets displayed that the nanosheets were composed of carbon and nitrogen elements. And it also proved that the atomic ratio of carbon and nitrogen was 3 to 4, verified that the g-C_3N_4 was successfully synthesized in this work, which was prepared for the further use.

Fig. 3 displayed the PEC response of the sensor in the absence and presence of Ch (1 μM). As we can saw, the photocurrent density at g-C_3N_4/GCE was higher than that at DZP/GCE which was so low that can be ignored, the excellent photocurrent benefited from the appealing electronic structure of g-C_3N_4 and the highly efficient conversion of light energy to electricity. However, after the hybrid of DZP and g-C_3N_4 was dropped onto the electrode surface, the photoelectrochemical performance enhanced dramatically, as demonstrated in Fig. 4A, B and C. It strongly proved that the present of DZP could overcome the large activation barrier during short period, allowing the light-initiated reactivity by the conversion of the light energy into chemical energy. The finding results from two aspects, on one hand, the g-C_3N_4 was functionalized spontaneously by dendritic phthalocyanine with the carboxylic groups, which acted as an energy absorbing and electron transferring antenna to enhance the PEC response to visible light. DZP was coupled with g-C_3N_4 nanosheets through axial coordination, where nitrogen in g-C_3N_4 as Lewis base showed high adsorption capacity for the zinc ion of DZP. Then the spatial structure of distortion of DZP was distorted, leading to the spatial charge separation of photo-generated charge carrier. In addition, there was electrostatic repulsive force between the electronegative g-C_3N_4 and DZP. The interaction led to supermolecular ring distorted further, the Lewis acidity of the Zn ion in DZP became stronger, leading to the stronger axial coordination between g-C_3N_4 and DZP. Therefore an electron donor-acceptor assembly was constructed, resulting in achieving high efficiency and long lifetime the charge separation of photo-generated carriers. On the other hand, the energy levels of the LUMO and HOMO of DZP just could match with that of g-C_3N_4 nanosheets, which interdicted the recombination of the electron-hole pairs. Thus it could be employed as potential sensitizer for the pholoelectrochemical application of the g-C_3N_4.

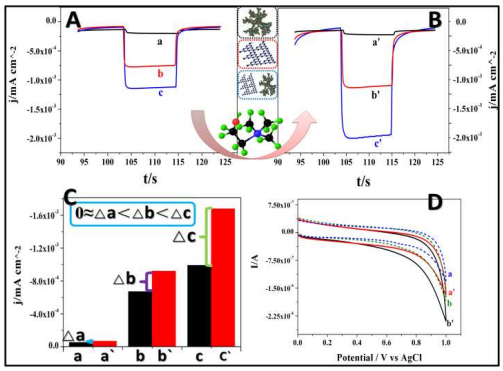

Fig.3 (A) The photocurrent response of various modified electrodes (a) DZP/GCE, (b)g-C_3N_4/GCE, (c)g-C_3N_4/DZP/GCE in 0.1M PBS (pH 7.0), (B) The photocurrent response of various modified electrodes in 0.1 M PBS (pH 7.0) containing 1 μM Ch, (C) The photocurrent density contrasting pattern of different electrodes in 0.1 M PBS (pH 7.0) and 1 μM Ch solution, (D) CV curves of the g-C_3N_4/DZP/GCE in the absence (a), (a') and (b), (b') present of 1 μM Ch, and (a'), (b') with irradiation, (a), (b) without irradiation.

The contrasting pattern in Fig. 3C showed the photocurrent density at various modified electrodes in the solution containing Ch was higher than that in the blank PBS. Since Ch acted as the effective electron donor for scavenging holes, and the recombination of electron-hole was inhibited, then the photocurrent intensity enhanced dramatically. The cyclic

voltammogram of the g-C_3N_4/DZP electrode, as Fig. 3D demonstrated, did not display obviously oxidation peaks in the potential range from 0 to 1.0 V in the presence and absence of 1 μM Ch containing 0.1M PBS (pH=7) solution, which suggested Ch could not be oxidized under this condition. However, the CV profile increased in the present of Ch under irradiation due to the Ch oxidation caused by the holes on the g-C_3N_4. The phenomenon was consistent with that above. Therefore, g-C_3N_4/DZP axial coordinated composites have potential applications in PEC sensors.

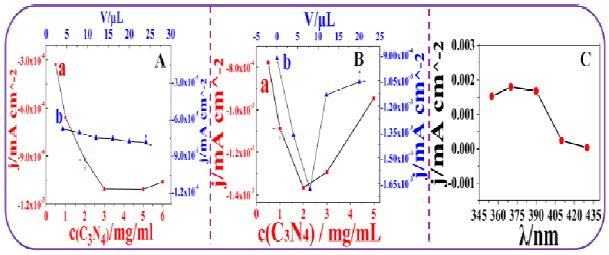

Fig. 4 (A) the effect of amount of g-C_3N_4 at g-C_3N_4/GCE (a) , the effect of amount of DZP at DZP/GCE, (B) the effect of amount of g-C_3N_4at g-C_3N_4/DZP/GCE(a), the effect of amount of DZP at g-C_3N_4/DZP/GCE, (C) excitation wavelength on photocurrent responses of g-C_3N_4/DZP/GCE in 0.1 M PBS (pH 7.0) containing 1 μM choline.

In order to optimize the experimental conditions for Ch detection, the effects of the amount of g-C_3N_4 and DZP and the excitation wavelength were investigated. As depicted in Fig. 4A, the photocurrent enhanced obviously with the increasing amount of g-C_3N_4 on the g-C_3N_4 modified electrode. When the g-C_3N_4 amount beyond 3 mg mL^{-1}, the photocurrent decreased, resulting from the molecular aggregation by large π-conjugation blocked the photo-generated electron transfer. As Fig. 4A illustrated, the effect of DZP amount on the photo-current of modified electrode depicting the photocurrent almost did not change with the amount of DZP, which strongly proved the photocurrent was generated by g-C_3N_4, and DZP just acted as sensitizer for g-C_3N_4. Additionally, the amount of g-C_3N_4 and DZP on the g-C_3N_4/DZP/GCE was optimized for choline measurement. As described in Fig. 4B, the photocurrent on the g-C_3N_4/DZP electrode substantially increased with the increased amount of g-C_3N_4 from 0 to 2 mg mL^{-1} (curve a), then it decreased quickly afterward. Then the curve b in Fig. 4B depicted that the photoelectrochemical response enhanced with the amount of DZP increasing from 0 to 8 μL, beyond that it decreased dramatically. Therefore, 2 mg mL^{-1} of g-C_3N_4 and 8 μL DZP solutions were chosen for the further study. The irradiation wavelength was one of significant factors which quite relevant to the photocurrent response. As displayed in Fig. 4C, in the choline solution, the photocurrent density increased as the exciting wavelength was increased from 355 nm to 375 nm, subsequently, the photocurrent density was decreased only a little from 375nm to 390nm, then it dramatically decreased beyond 390 nm. The exciting wavelength of 390 nm was in the range of visible light, so it was chosen for the photoelectrochemical determination of choline.

Under the optimum experimental conditions (Fig. 4), the operational stability of the sensor was displayed in Fig. 5A. The relative standard deviation for ten parallel measurements with g-C_3N_4/DZP modified electrode was 4.3%, indicating an excellent precision. Moreover, the reproducibility of the sensor was estimated by detection 1 μM Ch with ten biosensors prepared at the different electrodes. A relative standard deviation of 4.58% was attained from ten measurements, giving an acceptable fabrication reproducibility of the biosensor. Moreover, no evident descend in the photocurrent was observed after 15 days of storage at 4 ℃, implying that the fabricated sensor possessed good storage stability.

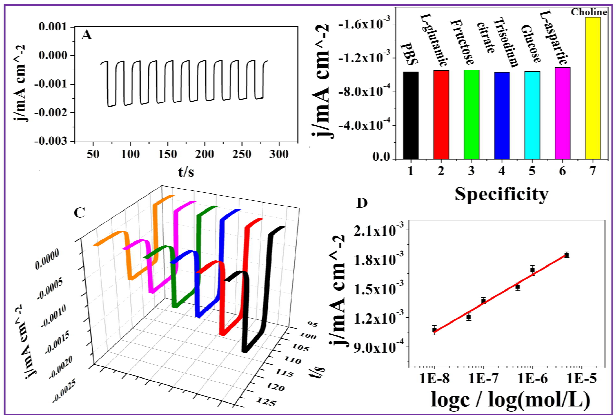

Fig. 5 (A) The stability of g-C_3N_4/DZP/GCE in 0.1 M PBS (pH 7.0) containing 1 μM Ch, (B) selectivity of PEC biosensor for 0.1M PBS, 100 μM L-glutamic, Fructose, Trisodium citrate, Glucose, L-aspartic and 1μM Ch, (C) effect of the concentration of Ch 0.01 μM, 0.05 μM, 0.1 μM, 0.5 μM, 1 μM, 5 μM. (D) The plot of photocurrent density against the logarithm of concentration of Ch.

As Fig. 5B revealed, the present biosensor showed an excellent selectivity for Ch over the other agents. To further demonstrate the analytical reliability and real application of the PEC biosensor, the quantitative determination of Ch was developed, as the Fig. 5C displayed. Hence, by tracking the photocurrent density related to the logarithm of concentration of Ch (Fig. 5D) the curve had a linear range from 10 nM to 5 μM and the detection limit was 3 nM, which was lower than other Ch sensors.[28-32] The prepared biosensor was used for detecting the trace amount of Ch in practical analytical applications as it shown in Table S2.

In summary, an enzyme free PEC sensing scaffold based on the axial coordinated g-C_3N_4/DZP composites was presented. In this scaffold, by coupling the unique textural and electronic features of g-C_3N_4 with dendritic phthalocyanine through axial coordination, the high charge separation efficiency could be obtained owing to the block of recombination of the electron-hole pairs, Ch was firstly introduced in this analytical system which acted as an effective electron donor, further generated the amplified photocurrent. The fabrication of the biosensor which possesses high sensitivity, good reproducibility and long-term stability marked a starting point for further research in this field based on g-C_3N_4 nanosheets, offering the possibility of coupling g-C_3N_4 nanosheets with dendritic phthalocyanine in potential

application including photoelectroanalysis, photocatalytic degradation and etc.

This project was financially supported by NSFC (21205016, 21275031, 21274021), National Science Foundation of Fujian Province (2011J05020), Education Department of Fujian Province (JA14071, JB14036, JA13068), Foundation of Fuzhou Science and Technology Bureau (2013-S-113) and Fujian Normal University outstanding young teacher research fund projects (fjsdjk2012068).

Notes and references

[a] *College of Chemistry and Chemical engineering , Fujian Normal University, Fuzhou, Fujian, 350108,China*
E-mail: dhong@fjnu.edu.cn (H. Dai); gnchen@fzu.edu.cn (G. Chen); Fax: (+86)-591-22866135
[b] *MOE Key Laboratory and Fujian Provincial Key Laboratory for Analysis and Detection for Food Safety, and Department of Chemistry, Fuzhou University, Fuzhou, Fujian 350002, China*
† Electronic Supplementary Information (ESI) available: experimental details. See DOI: 10.1039/b000000x/

1 D. Chen, H. Zhang, X. Li and J. Li, *Anal. Chem*., 2010, **82**, 2253;
2 R. Gill, M. Zayats and I. Willner, *Angew. Chem. Int. Ed.*, 2008, **47**, 7602.
3 X. M. Zhao, S. W. Zhou, Q. M. Shen, L. P. Jiang and J. J. Zhu, *Analyst* 2012, **137**, 3697;
4 W. W. Zhao, Z. Y. Ma, P. P. Yu, X. Y. Dong, J. J. Xu and H. Y. Chen, *Anal. Chem.* 2012, **84**, 917;
5 W. J. Wang, J. P. Lei, W. W. Tu and H. X. Ju, *Anal. Chim. Acta* 2012,**744**, 33;
6 M. Liang, S. Jia, A. Zhu and L. Guo, *Environ. Sci. Technol.* 2008, **42**, 635;
7 Y. J. Li, M. J. Ma and J. J. Zhu, *Anal. Chem*. 2012, **84**, 10492.
8 P. P. Wang, W. J. Dai, L. Ge, M. Yan, S. G. Ge and Yu, J. H. *Analyst* 2013, **138**, 939;
9 Q. M. Shen, X. M. Zhao, S. W. Zhou, W. H. Hou and J. J. Zhu, *J. Phys. Chem. C*. 2011, **115**, 17958;
10 Yao, W. J.; Alan, L. G.; Nicolas, S.; Michael, H.; Guo, W. D.; Dan, S.; Eric, D.; Serge, C. *Biosens. Bioelectron.* 2013, **42**, 556.
11 C. M. Cheng, Y. Huang, X. Q. Tian, B. Z. Zheng, Y. Li, H. Y. Yuan, D. Xiao, S. P. Xie and M. M. Choi, *Anal. Chem.* 2012, **84**, 4754;
12 X. S. Zhou, B. Jin, R. Q. Chen, F. Peng and Y. P. Fang, *Mater. Res. Bull.* 2013, **48**, 1447.
13 B. Chai, T. Y. Peng, J. Mao, K. Li and L. Zan, *Phys. Chem. Chem. Phys.* 2012, **14**, 1674.
14 L. P. Zhang and Z. H. Xia, *J. Phys. Chem. C.* 2011, **115**, 11170.
15 M. Wu, C. Cao and J. Z. Jiang, *Nanotechnology* 2010, **21**, 505202.
16 H. B. Wang, T. Maiyalagan and X. Wang, *ACS Catal.* 2012, **2**, 781-794.
17 J. Q. Tian, Q. Liu. C. J. Ge, Z. C. Xing, A. M. Asiri, A. O. Al-Youbi and X. P. Sun, *Nanoscale* 2013, **5**, 8921;
18 N. Karousis, J. Ortiz, K. Ohkubo, T. Hasobe, S. Fukuzumi, A. S. Santos and N. Tagmatarchis, *J. Phys. Chem. C* 2012, **116**, 20564.
19 C. Ingrosso, A. Petrella, P. Cosma, M. L. Curri, M. Striccoli and A. Agostiano, *J. Phys. Chem. C.* 2006, **110**, 24424.
20 Y. R. Peng, H. Zhang, H. L. Wu, B. Q. Huang, L. Gan, and Z. Chen, *Dyes Pigment.* 2010, **87**, 10.
21 H. Q. Yang, Y. R. Peng, L. Sh. Huang, H. Zhang, Y. H. Wang and Xie, S. S. *J. Lumin.* 2013, **135**, 26.
22 S. Fukuzumi, T. Honda, K. Ohkubo and Ta. Kojima, *Dalton Trans.* 2009, **20**, 3880.
23 B. K. Chandra, K. Ohkubo, P. A. Karr, S. Fukuzumi and F. D. Souzaa, *Chem. Commun.* 2013, **49**, 7614.
24 M. M. Liu, R. Liu and W. Chen, *Biosens. Bioelectron.*, 2013, **45**, 206.
25 X. J. Zhang, L. J. Mao, D. Zhang and L. Zhang, *J. Mol. Struct*., 2012, **1022**, 153.
26 B. H. Meekins and P. V. Kama, *ACS NANO* 2009, **11**, 3437.
27 N. Karousis, J. Ortiz, K. Ohkubo, T. Hasobe, S. Fukuzumi, A. S. Santos and N. Tagmatarchis, *J. Phys. Chem. C* 2012, **116**, 20564.
28 C. Z. Zhao, J. Yu, G. S. Zhao and K. Jiao, *Anal. Chem.* 2011, **39**, 886.
29 Z. Arie, G. Miri, and B. Juan, *CHEMPHYSCHEM,* 2003, **4**, 859.
30 S. Çevik, S. Timur and Ü. Anik, *Microchim. Acta*., 2012, **179**, 299.
31 H. Dai, X. P.Wu, H. F. Xu, M. D. Wei, Y. M. Wan and G. N. Chen, *Electrochem. Commun.* 2009, **11**, 1599.
32 Y. N. Li, H. Huang, F. P. Shi, Y. Li and X. G. Su, *Microchim. Acta.*, 2013, **180**, 1135.

A table of contents entry

High photoactive heterojunction based on g-C_3N_4 and dendritic zinc (Ⅱ) phthalocyanine was firstly proposed for the ultrasensitive detection of choline.